

Tackling the SARS-Cov-2 main protease using hybrid derivatives of 1,5-disubstituted tetrazole-1,2,3-triazoles: an *in silico* assay

Carlos J. Cortés-García^{Equal first author, 1}, Luis Chacón-García¹, Jorge Emmanuel Mejía-Benavides², Erik Díaz-Cervantes^{Corresp. Equal first author, 3}

¹ Laboratorio de Diseño Molecular / Instituto de Investigaciones Químico-Biológicas / Universidad Michoacana de San Nicolás de Hidalgo, Universidad Michoacana de San Nicolás de Hidalgo, Morelia, Michoacán, Mexico

² Departamento de Enfermería y Obstetricia / Centro Interdisciplinario del Noreste (CINUG), Universidad de Guanajuato, Tierra Blanca, Guanajuato, Mexico

³ Departamento de Alimentos / Centro Interdisciplinario del Noreste (CINUG), Universidad de Guanajuato, Tierra Blanca, Guanajuato, Mexico

Corresponding Author: Erik Díaz-Cervantes

Email address: e.diaz@ugto.mx

In regard to the actual public health global emergency and, based on the state of the art about the ways to inhibit the SARS-Cov-2 treating the COVID19, a family of 1,5-disubstituted tetrazole-1,2,3-triazoles, previously synthesized, have been evaluated through *in silico* assays against the main protease of the mentioned virus (Cov-2-M^{Pro}). The results show that three of these compounds present a more favorable interaction with the selected target than the co-crystallized molecule, which is a peptide-like derivative. It was also found that also hydrophobic interactions play a key role in the ligand-target molecular couplings, due to the higher hydrophobic surfaces into the active site. Finally, a pharmacophore model has been proposed based on the results below, and a family of 1,5-DT derivatives has been designed and tested with the same methods employed in this work. It was concluded that the compound with the isatin as a substituent (P8) present the higher ligand-target interaction, which makes this a strong drug candidate against COVID19, due can inhibit the Cov-2-M^{Pro} protein.

Tackling the SARS-Cov-2 main protease using hybrid derivatives of 1,5-disubstituted tetrazole-1,2,3-triazoles: an *in silico* assay

Carlos J. Cortes-García³, Luis Chacón- García³, Jorge Emmanuel Mejía-Benavides², Erik Díaz-Cervantes^{1*}

¹Departamento de Alimentos, ²Departamento de Enfermería y Obstetricia, Centro Interdisciplinario del Noreste (CINUG), Universidad de Guanajuato, 37975 Tierra Blanca, Guanajuato, México

³Laboratorio de Diseño Molecular, Instituto de Investigaciones Químico-Biológicas, Universidad Michoacana de San Nicolás de Hidalgo. Ciudad Universitaria, C.P. 58033, Morelia, Michoacán, México

Corresponding Author:

Erik Díaz-Cervantes¹

Universidad de Guanajuato, 37975 Tierra Blanca, Guanajuato, México

Email address: e.diaz@ugto.mx

Abstract

In regard to the actual public health global emergency and, based on the state of the art about the ways to inhibit the SARS-Cov-2 treating the COVID19, a family of 1,5-disubstituted tetrazole-1,2,3-triazoles, previously synthesized, have been evaluated through *in silico* assays against the main protease of the mentioned virus (Cov-2-M^{Pro}). The results show that three of these compounds present a more favorable interaction with the selected target than the co-crystallized molecule, which is a peptide-like derivative. It was also found that also hydrophobic interactions play a key role in the ligand-target molecular couplings, due to the higher hydrophobic surfaces into the active site. Finally, a pharmacophore model has been proposed based on the results below, and a family of 1,5-DT derivatives has been designed and tested with the same methods employed in this work. It was concluded that the compound with the isatin as a substituent (P8) present the higher ligand-target interaction, which makes this a strong drug candidate against COVID19, due can inhibit the Cov-2-M^{Pro} protein.

I. Introduction

Recently, a new kind of coronavirus strain was discovered in Wuhan city in Hubei province, central China, known as severe acute respiratory syndrome coronavirus 2 (SARS-CoV-2) causing the coronavirus disease 2019 (COVID-19), which has now become a pandemic threat (Gabutti et al. 2020; Gralinski & Menachery 2020; Jin et al. 2020). At present, SARS-CoV-2 has caused thousands of deaths and more than 1.5 million people have been infected worldwide, becoming a global public health emergency (Sohrabi et al. 2020). Despite there are no specific antivirals for a treat the COVID-19, the scientific community is using the drug repurposing of some FDA drugs approvals such as lopinavir, remdesivir, and chloroquine as a rapid strategy to find a cure (Kandeel & Al-Nazawi 2020; Li & Clercq 2020; Li et al. 2020; Shah et al. 2020), but the need to develop a new specific antiviral drug is still urgent.

Thus, a quick and efficient way to find a new drug candidate is through computer-aided drug design (CADD) which is a powerful tool used to find new leads compound by reducing risk, time, and cost of research in drug discovery research (Baig et al. 2016; Bisht & Singh 2018; Ferreira et al. 2015; Hoque et al. 2017). Moreover, in February 2020, the first high-resolution crystal structure of the main protease of SARS-CoV-2 (PDB code: 6lu7) (Liu et al. 2020b), which is related to the viral life cycle was published, making it a key target to develop some new antiviral agents.

Moreover, based on the main protease of SARS-CoV-2 (Cov-2-M^{Pro}), which presents a similar structure to the M^{Pro} of the SARS-Cov (He et al. 2020; Liu et al. 2020a; Vellingiri et al. 2020), note that the hydrogen bonds are the reported interactions as the main between the ligand and the target (Chou et al. 2003). Also, searching in the state of the art about the potential candidates to target his specific enzyme it was found that some 1,2,3-triazoles synthesized by the Dehaen group were evaluated as potential anti-coronavirus agents (Karypidou et al. 2018). In this context, the present work aimed to evaluate in silico a series of 1,5DT derivatives which were previously synthesized in our research group (Aguilar-Morales et al. 2019) and whose biological and theoretical essays have not been reported.

Therefore, based on the remarkable recent results about the different kind of molecules that can interact with the selected target (Cov-2-M^{Pro}), ranging from molecules from medicinal plants (Qamar et al. 2020) and other plants with known health properties, as the garlic (Phuong-Thuy et al. 2020), since the use of alpha ketoamide as inhibitors of this biological target (Zhang et al. 2020), in the present work, has been proposed the above mentioned 1,5-disubstituted tetrazole-1,2,3-triazoles as a novel plausible inhibitors of the Cov-2-M^{Pro}.

II. Computational Methods

The Cartesian coordinates from the selected target, Cov-2-M^{Pro}, were obtained from the protein data bank (PDB code: 6lu7), which was one of the first crystallized structures of the main protease of the SARS-Cov-2 virus. Furthermore, the Chimera package was used to add charges, remove solvents and correct residues of the target structure (Pettersen et al. 2004).

Moreover, the 1,5-disubstituted tetrazole-1,2,3-triazoles, see **Fig. 1**, which are considered as ligands, were modeled using the Avogadro software (Jin et al. 2020) and charged with the Chimera package (Pettersen et al. 2004). However, to obtain a better approach, the ligands were optimized at the UFF level (Rappe et al. 1992) using the Gaussian 09 (G09) package (Frisch et al. 2009).

On the other hand, the ligand-target interactions were obtained using the Molegro MVD package and the *in silico* molecular couplings, so-called molecular *docking*, were performed through the MolDock score function (Thomsen & Christensen 2006). Also, the electrostatic, hydrogen bond and hydrophilic surfaces interactions were obtained with the same MVD software.

Finally, the pharmacophore model was performed using the ZINCPharmer server (Koes & Camacho 2012), considering the obtained properties throughout the whole study. It is noteworthy to mention that the proposed novel inhibitors carried out the same process as the 1,5-disubstituted tetrazole-1,2,3-triazoles and have been evaluated in the selected target with the above method.

III. Results and Discussion

3.1 Add Docking results

The results obtained using the above methods in regard to the *in silico* molecular couplings are presented in this section. The specific docking of all the modeled ligands, see **Fig. 1**, into the active site of the protein Cov-2-M^{Pro} is shown in **Fig. 2**, which exposes that all the ligands docked similarly to the selected target interacted with the catalytic triad residues, which will be explained below.

To evaluate the best ligand docked in the selected target, COV2-M^{Pro}, the MolDock score energy was considered as a parameter of measurement. Furthermore, the ligand efficiency (LE = Energy/No. of heavy atoms) was used to determine with better precision the ligand-target binding strength. This parameter gives the energy provided per atom to the ligand-target interaction, making it a better comparison between ligands with different number of atoms.

Table 1 shows the energies, hydrogen bond, and electrostatic interactions, as well as the LE values obtained for the selected ligands.

In comparison with the co-crystallized ligand reported in the PDB file, **1e** is 0.04 kcal/mol more stable (Liu et al. 2020b). Also, P8 is the molecule with higher ligand as well as, P8 is the molecule with the higher ligand-target interaction energy.

Moreover, the hydrogen bond (H_{bond}), electrostatic (Elstat) interactions and the Van der Waals energies (VdW) are shown in **Table 1**, being the VdW the limiting energy to obtain a better ligand-target interaction for this kind of systems because the best ligands present the most favorable VdW energy. However, the state of the art regarding this protease indicates that the hydrogen bond interactions are one of the most important energies, especially with the amides of the catalytic triad residues (Gly143, Cys145, and Ser144)(Zhang et al. 2020). Note that table 1 includes compounds P1-10, which are the designed potential inhibitors presented in this work and will be boarded in section 3.3

In respect to the docked cavity, our results accord with the obtained by other authors, shown the interactions of the ligands into the active site of the protein, so-called catalytic triad (Gly143, Ser144, and Cys145), see **Fig. 3**. At the same time, the His41 and the Asp187 are important ligands to begin the electronic transfer. Are important ligands at the onset of the electronic transfer, which is the key mechanism in peptide bond rupture for this kind of protease. Other key fragments in the oxyanion hole include Gly143 and SER144, which according to Warshel and co-workers(Kamerlin et al. 2010; Mukherjee & Warshel 2012), stabilize. This helps identify the active site and is a way to corroborate that this cavity is the target site of the protein.

Fig. 3 shows first the co-crystallized molecule (a peptide like derivative) which directly interacts with the catalytic triad and part of the molecule dock perfectly in almost the whole cavity. However, **Fig. 3B** depicts the two best ligands interacting in a similar way than the co-crystallized molecule, but filling the right site of the computed cavity, this behavior of the ligands can be the reason of the most favorable interactions for these, comparing with the co-crystallized molecule, see **Table 1**.

3.2 Hydrogen bonds and electrostatic interactions

The **1e** ligand, which is the compound with the most favorable ligand-target interactions, considering the ligand efficiency and the binding energy, presents hydrogen bond interactions with Ser144 and His164, see **Fig. 4A**. Note that these are residues of the catalytic site. Furthermore, **Fig 4B** shows the same ligand interacting with His41, His163, Glu166, and His172 via electrostatic forces, in which the repulsive electrostatic interactions are more prominent than the attractive ones. This kind of interaction plays a key role in the final conformation of the

bioactive posse. Generally, the electrostatic interactions are one of the limiting energies in the ligand-target coupling and ligand 1e shows a value of -0.65, being this one of the highest ones of the table.

3.3 Hydrophobic interactions

To better evaluate the ligand-target interactions, it is necessary to carry out an analysis of the hydrophobic surfaces of the selected cavity. The hydrophobicity surfaces of the active site show that in the deep zone of the cavity a hydrophobic zone can be found, as shown in Fig 5 in blue colored surfaces. However, the front of the cavity and one site in the upper-left zone shows a higher hydrophilic site, depicted in red color in **Fig. 5**.

Fig 5A shows the interactions between the co-crystallized ligand and the selected target, from a viewing a hydrophobic behavior. How the ligand takes a conformation into the cavity occupying only the deep zone of the active site (the more hydrophobic site) and avoids the interactions with the front of the cavity. Note that, this similar behavior shows the ligand 1e when this interacts with the active site, see **Fig. 5B**.

Even though ligand 1e interacts in the Deep side of the cavity, it docked less in the left site of the surface, and do not cross the cavity space in the right site, as did the co-crystallized. Note that ligand 1e presents higher L.E., than the co-crystallized ligand, see **Table 1**. Therefore, it is clear that the presence of aromatic and hydrophobic rings in both molecules is essential and key for better interactions, and the hydrophilic interactions are directly negligible.

3.4 Pharmacophore model

Based on the whole results, specially the docking results obtained by the 1e ligand and the co-crystallized ligand and taken the hydrophobic surfaces as one of the main interactions, a pharmacophore model was performed. The principal aim in developing this model was to predict and propose which molecular fragments are necessary to interact with COV-2MA, which would result in virus inhibition.

The proposed pharmacophore model is shown in **Fig. 6**, which consists of ten principal components: two hydrophobic fragments (Hy, depicted in green color), one aromatic fragment (Ar, colored in blue color), three hydrophobic-aromatic fragments (Hy-Ar, represented in purple color), two hydrogen donor fragments (HD, depicted in gray color) and two hydrogen acceptor fragments (colored in orange color). Analyzing **Fig6**, it is clear that the low side of the model needs mostly hydrophobic fragments, and in the top, the fragments are HD and HA.

3.5 Proposing molecules

Based on the obtained results and considering the pharmacophore model, a series of ten 1,5-disubstituted tetrazole-1,2,3-triazoles have been proposed as inhibitors of the Cov-2-M^{Pro}, which are depicted in **Fig. 7**. As shown in **Table 1**, the P8 and P10 designed molecules present the more favorable interactions with the selected target, presenting a more negative LE respect to the other evaluated compounds. Note that, six of the ten designed molecules present better interaction with the Cov-2-M^{Pro} than the co-crystallized molecules, which is the reference molecule.

On the other hand, the P8 compound has in its structure the molecule so-called isatin or 1H-indole-2,3-dione, which is considered as a privileged scaffold because its derivate possesses broad biological and pharmacological activity including antibacterial, anticancer, antitubercular, antimalarial, antifungal, anticancer, anti-HIV, and in general antiviral (Varun et al. 2019). This Analyzing the bio-active possess of compound P8, it is seen that it promotes an intramolecular stabilization due to two stacking interactions, interacting with the triazole ring and the benzene ring, face-to-edge, and face-to-face, respectively.

However, **Fig. 8A** shows that the P8 molecule prefers to interact in the right side of the molecule and with a Similarly to the co-crystallized ligand and the 1e compounds, the structure of compound P8 is located in the deep of the active site. Note that the principal hydrophobic interactions between P8 and the Cov-2-M^{Pro} are with blue surfaces, which represent the hydrophobic site in the cavity. These results can be explained by the higher quantity of rings in the P8 structures, which can promote hydrophobic interactions.

In the case of the hydrogen bond interactions, P8 molecule interacts not only with the catalytic triad, specify with the Ser 144 and Cys145, but presents a higher number of interactions with other residues that include Ser1 and Asn 142. The last one promotes higher H_{bond} energy, see **Table 1** than compound 1e. Highlights the results reported in the state of the art about the Cov-2-M^{Pro} (Liu et al. 2020b), hydrogen bond interactions play a key role in the ligand-target interaction. Moreover, the electrostatic interactions between P8 and the selected target take place at the residues His41, His163, Glu166, and His172, which in terms of Elstat energy, do not help to grow the favorable interaction.

On the other hand, the best interacting molecules both the previously synthesized (1e) by some of us and the designed in this work (P8) have been evaluated into the pharmacophore model and analyze through the segments docked with the proposed structure. **Fig. 9A** shows the molecule 1e in the pharmacophore model, which reveals that this molecule needs some components to

complete all the pharmacophore fragments, specifically, it needs an aromatic moiety, as well as an HD and HA fragments in the top of the molecule.

Finally, **Fig. 9B** depicts the P8 structure into the pharmacophore model and shows that this molecule needs only two fragments to complete all the requirements of the pharmacophore model, which are a Hy and one HD fragments. Analyzing the results, it is clear that to obtain a better molecule that could inhibit the Cov-2-M^{Pro} it is necessary to have a system that includes some rings in their structure. Also, the right side of the cavity is more important, as long as the size of the molecule does not overpass the size of the cavity or, in this case, the size of the pharmacophore model.

IV. Conclusions

A family of compounds previously synthesized by some of us was tested to inhibit the protein Cov-2-M^{Pro}, the results show that three of these compounds present a more favorable interaction with the selected target than the co-crystallized molecule, which is a peptide-like derivative. Moreover, although the fact that hydrogen bond interactions are mentioned in the state of the art about the selected protease, it can also be found that the electrostatic interactions and main the hydrophobic interactions play a key role in the ligand-target molecular couplings.

At the same time, the results reveal that a molecule can couple into the active site, which presents higher hydrophobic surfaces. and Thus, increasing the need to synthesize a molecule with a higher number of aromatic rings and their structures. Note that the residues of the active site interact in a stronger way with the best ligand coupled.

Finally, a pharmacophore model has been designed, which was used to propose a new family of 1,5-disubstituted tetrazole-1,2,3-triazoles derivatives which are candidates to be synthesized as a perspective of this work. Based on the obtained results, the best ligands were coupled with the pharmacophore model, which highlights a derivative with the isatin moiety were tested into the pharmacophore model in which derivatives bearing the isatin substituent shown a higher potential in the design of new drugs against the SARS-Cov-2. Hydrophobic and stacking interactions also play a key role in the design of new drug candidates to treat the COVID19.

Acknowledgements

We are grateful to the Laboratorio Nacional de Caracterización de Propiedades Fisicoquímicas y Estructura Molecular (UG-UAA-CONACYT, Project: 123732) for the computing time provided. E. Díaz-Cervantes acknowledge to the SICES by the support in the project: IJ-19-77 (Programa de empuje científico y tecnológico modalidad “Apoyo a Investigadores Jóvenes”), also acknowledge to Citlalli, Emily and Naomi.

Competing Interests

The authors declare that they have no competing interests

References

- Aguilar-Morales CM, Loera Dd, Contreras-Celedón C, Cortés-García CJ, and Chacón-García L. 2019. Synthesis of 1,5-disubstituted tetrazole-1,2,3 triazoles hybrids via Ugi-azide/CuAAC. *Synth Commun* 49:2086-2095. <https://doi.org/10.1080/00397911.2019.1616301>
- Baig MH, Ahmad K, Roy S, Ashraf JM, M MA, Siddiqui MH, Khan S, Kamal MA, Provazník I, and Choi I. 2016. Computer Aided Drug Design: Success and Limitations. *Curr Pharm Design* 22:572-581. <http://https://doi.org/10.2174/1381612822666151125000550>
- Bisht N, and Singh BK. 2018. ROLE OF COMPUTER AIDED DRUG DESIGN IN DRUG DEVELOPMENT AND DRUG DISCOVERY. *Int J Pharm Sci Res* 9:1405-1415. [http://dx.doi.org/10.13040/IJPSR.0975-8232.9\(4\).1405-15](http://dx.doi.org/10.13040/IJPSR.0975-8232.9(4).1405-15)
- Chou K-C, Wei D-Q, and Zhong W-Z-. 2003. Binding mechanism of coronavirus main proteinase with ligands and its implication to drug design against SARS. *Biochem Biophys Res Commun* 308:148-151. <http://doi.10.1016/j.bbrc.2003.09.053>
- Ferreira LG, Santos RNd, Oliva G, and A. D. Andricopulo. 2015. Molecular Docking and Structure-Based Drug Design Strategies. *Molecules* 20:13384-13421. <https://doi.org/10.3390/molecules200713384>
- Frisch MJ, Trucks GW, Schlegel HB, Scuseria GE, Robb MA, Cheeseman JR, Scalmani G, Barone V, Mennucci B, Petersson GA, Nakatsuji H, Caricato M, Li X, Hratchian HP, Izmaylov AF, Bloino J, Zheng G, Sonnenberg JL, Hada M, Ehara M, Toyota K, Fukuda R, Hasegawa J, Ishida M, Nakajima T, Honda Y, Kitao O, Nakai H, Vreven T, Jr. JAM, Peralta JE, Ogliaro F, Bearpark M, Heyd JJ, Brothers E, Kudin KN, Staroverov VN, Kobayashi R, Normand J, Raghavachari K, Rendell A, Burant JC, Iyengar SS, Tomasi J, Cossi M, Rega N, Millam JM, Klene M, Knox JE, Cross JB, Bakken V, Adamo C, Jaramillo J, Gomperts R, Stratmann RE, Yazyev O, Austin AJ, Cammi R, Pomelli C, Ochterski JW, Martin RL, Morokuma K,

- Zakrzewski VG, Voth GA, Salvador P, Dannenberg JJ, Dapprich S, Daniels AD, Farkas Ö, Foresman JB, Ortiz JV, Cioslowski J, and Fox DJ. 2009. Gaussian 09. C.01 ed: Wallingford CT.
- Gabutti G, d'Anchera E, Sandri F, Savio M, and Stefanati A. 2020. Coronavirus: Update Related to the Current Outbreak of COVID-19. *Infect Dis Ther*. <https://doi.org/10.1007/s40121-020-00295-5>
- Gralinski LE, and Menachery VD. 2020. Return of the Coronavirus: 2019-nCoV. *Viruses* 12:135. <https://doi.org/10.3390/v12020135>
- He J, Tao H, Yan Y, Huang S, and Xiao Y. 2020. Molecular Mechanism of Evolution and Human Infection with SARS-CoV-2. *Viruses* 12:428. <https://doi.org/10.3390/v12040428>
- Hoque I, Chatterjee A, Bhattacharya S, and Biswas R. 2017. An Approach of Computer-Aided Drug Design (CADD) Tools for In Silico Pharmaceutical Drug Design and Development. *Int J Adv Res Biol Sci* 4:60-71. <http://dx.doi.org/10.22192/ijarbs.2017.04.02.009>
- Jin Y, Yang H, Ji W, Wu W, Chen S, Zhang W, and Duan G. 2020. Virology, Epidemiology, Pathogenesis, and Control of COVID-19. *Viruses* 12:322. <https://doi.org/10.3390/v12040372>
- Kamerlin SCL, Chu AT, and Warshel A. 2010. On Catalytic Preorganization in Oxyanion Holes: Highlighting the Problems with the Gas-Phase Modeling of Oxyanion Holes and Illustrating the Need for Complete Enzyme Models. *J Org Chem* 75:6391-6401. <https://doi.org/10.1021/jo100651s>
- Kandeel M, and Al-Nazawi M. 2020. Virtual screening and repurposing of FDA approved drugs against COVID-19 main protease. *Life Sci*. <https://doi.org/10.1016/j.lfs.2020.117627>
- Karypidou K, Ribone SR, Quevedo MA, Persoons L, Pannecouque C, Helsen C, Claessens F, and Dehaen W. 2018. Synthesis, biological evaluation and molecular modeling of a novel series of fused 1,2,3-triazoles as potential anti-coronavirus agents. *Bioorg Med Chem Lett* 28:3472-3746. <https://doi.org/10.1016/j.bmcl.2018.09.019>
- Koes DR, and Camacho CJ. 2012. ZINCPharmer: pharmacophore search of the ZINC database *Nucleic Acids Res* 40:W409-W414. <https://doi.org/10.1093/nar/gks378>
- Li G, and Clercq ED. 2020. Therapeutic options for the 2019 novel coronavirus (2019-nCoV). *Nat Rev Drug Discov* 19:149-150. <https://doi.org/10.1038/d41573-020-00016-0>

- 358 Li H, Liu S, Yu X, Tang S, and Tang C. 2020. Coronavirus disease 2019 (COVID-19): current
359 status and future perspectives. *Int J Antimicrob Ag.*
360 <https://doi.org/10.1016/j.ijantimicag.2020.105951>
361
- 362 Liu C, Zhou Q, Li Y, Garner LV, Watkins SP, Carter LJ, Smoot J, Gregg AC, Daniels AD,
363 Jervey S, and Albaiu D. 2020a. Research and Development on Therapeutic Agents and Vaccines
364 for COVID-19 and Related Human Coronavirus Diseases. *ACS Cent Sci* 6:315-331.
365 <https://doi.org/10.1021/acscentsci.0c00272>
366
- 367 Liu X, Zhang B, Jin Z, Yang H, and Rao Z. 2020b. The crystal structure of COVID-19 main
368 protease in complex with an inhibitor N3. 2020-02-05 ed: Protein Data Bank.
369 <https://doi.org/10.2210/pdb6LU7/pdb>
370
371
- 372 Mukherjee S, and Warshel A. 2012. Realistic simulations of the coupling between the
373 protomotive force and the mechanical rotation of the F0-ATPase. *PNAS* 109:14876-14881.
374 <https://doi.org/10.1073/pnas.1212841109>
375
- 376 Pettersen EF, Goddard TD, Huang CC, Couch GS, Greenblatt DM, Meng EC, and Ferrin TE.
377 2004. UCSF Chimera--a visualization system for exploratory research and analysis. *J Comput*
378 *Chem* 25:1605-1612. <https://doi.org/10.1002/jcc.20084>
379
- 380 Phuong-Thuy BT, Ai-My TT, Thanh-Hai NT, Trung-Hieu L, Thai-Hoa T, Phuong-Loan HT,
381 Thanh-Triet N, Van-Anh TT, Tu-Quy P, Van-Tat P, Van-Hue N, Tuan-Quang D, Tien-Trung N,
382 Thanh-Tung V, Huynh LK, and Ai-Nhung NT. 2020. Investigation into SARS-CoV-2 Resistance
383 of Compounds in Garlic Essential Oil. *ACS Omega*. <https://doi.org/10.1021/acsomega.0c00772>
384
- 385 Qamar MTU, Alqahtani SM, Alamri MA, and Chen LL. 2020. Structural basis of SARS-CoV-2
386 3CLpro and anti-COVID-19 drug discovery from medicinal plants. *J Pharm Sci* 533.
387 <https://doi.org/10.1016/j.jpha.2020.03.009>
388
- 389 Rappe AK, Casewit CJ, Colwell KS, III WAG, and Skiff WM. 1992. *J Am Chem Soc*
390 114:10024-10035. <https://doi.org/10.1021/ja00051a040>
391
- 392 Shah B, Modi P, and Sagar SR. 2020. In silico Studies on Therapeutic Agents for COVID-19:
393 Drug Repurposing Approach. *Life Sci*. <https://doi.org/10.1016/j.lfs.2020.117652>
394
- 395 Sohrabi C, Alsafi Z, O'Neill N, Khan M, Kerwan A, Al-Jabir A, Iosifidis C, and Agha R. 2020.
396 World Health Organization declares global emergency: A review of the 2019 novel coronavirus
397 (COVID-19). *Int J Surg* 76:71-76. <https://doi.org/10.1016/j.ijsu.2020.02.034>

398

399 Thomsen R, and Christensen MH. 2006. MolDock: a new technique for high-accuracy molecular
400 docking. *J Med Chem* 49:3315-3321. <https://dx.doi.org/10.1021/jm051197e>

401

402 Varun, Sonam, and Kakkar R. 2019. Isatin and its derivatives: A survey of recent syntheses,
403 reactions, and applications. *Med Chem Commun* 10:351-368.
404 <https://doi.org/10.1039/C8MD00585K>

405

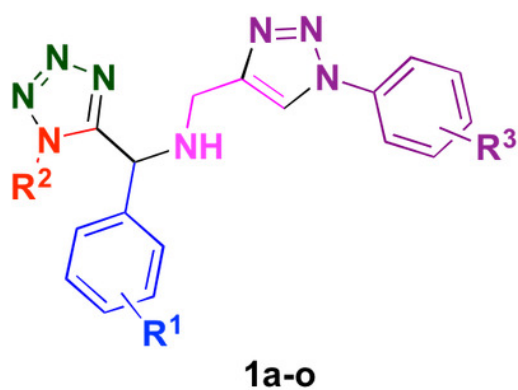
406 Vellingiri B, Jayaramayya K, Iyer M, Narayanasamy A, Govindasamy V, Giridharan B, Ganesan
407 S, Venugopal A, Venkatesan D, Ganesan H, Rajagopalan K, Rahman PK, Cho S-G, N. S.
408 Kumar, and Subramaniam MD. 2020. COVID-19: A promising cure for the global panic. *Sci*
409 *Total Environ* 725:138277. <https://doi.org/10.1016/j.scitotenv.2020.138277>

410

411 Zhang L, Lin D, Sun X, Curth U, Drosten C, Sauerhering L, Becker S, Rox K, and Hilgenfeld R.
412 2020. Crystal structure of SARS-CoV-2 main protease provides a basis for design of improved
413 α -ketoamide inhibitors. *Science*. <https://doi.10.1126/science.abb3405>

Figure 1

Modeled 1,5-disubstituted tetrazole-1,2,3-triazoles



Compound	R ¹	R ²	R ³
1a	H	<i>t</i> -Bu	4-CN
1b	4-F	<i>t</i> -Bu	4-CN
1c	4-Br	Cy	4-CN
1d	4-OMe	<i>t</i> -Bu	4-CN
1e	4-OMe	Cy	4-CN
1f	2-Cl	<i>t</i> -Bu	4-CN
1g	2-Br	Cy	4-CN
1h	2,4,5-triMe	<i>t</i> -Bu	4-CN
1i	H	Cy	4-Cl
1j	4-F	<i>t</i> -Bu	4-Cl
1k	4-Br	<i>t</i> -Bu	4-Cl
1l	4-OMe	<i>t</i> -Bu	4-NHCOMe
1m	4-OMe	Cy	4-NHCOMe
1n	4-Br	<i>t</i> -Bu	2-COPh-4Cl
1o	2-F	Cy	2-COPh-4Cl

Table 1 (on next page)

Interaction energies between the modeled ligands and the protein Cov-2-M^{Pro}.

All the units are represented in kcal/mol. H_{Bond} means the hydrogen bond interactions, Elstat the electrostatic energies, VdW indicates the Van der Waals energy and, LE is the ligand efficiency ($LE = E/\text{No heavy atoms}$).

Molecule	E	HBond	Electro	VdW	LE
P8	-255.79	-7.99	-0.11	-60.73	-5.44
P10	-210.29	-8.31	0.74	-56.38	-5.26
1e	-181.75	-2.52	-0.65	-52.43	-5.19
P7	-212.54	-6.86	0.05	-51.71	-5.18
1h	-174.15	-5.64	-0.45	-49.54	-5.12
P9	-213.61	-11.93	-0.38	22.42	-5.09
P6	-198.34	-8.17	0.03	-54.14	-5.09
P5	-198.33	-5.24	-0.72	-49.06	-5.09
1k	-157.03	-8.32	-0.54	-22.57	-5.07
Co-crystal	-211.79	-8.38	-0.61	-54.52	-5.04
1a	-155.38	-6.86	-0.10	-42.84	-5.01
P1	-215.37	-11.53	1.72	-66.12	-5.01
1j	-155.23	-5.05	-0.42	-44.01	-5.01
1g	-169.91	-6.86	0.58	53.31	-5.00
1i	-159.14	-10.08	0.09	-26.84	-4.97
P2	-213.91	-7.78	0.82	-34.42	-4.86
1m	-178.32	-0.82	-0.78	-38.11	-4.82
P3	-201.55	-13.36	-0.37	62.82	-4.80
1o	-193.90	-9.15	-0.09	-51.42	-4.73
1f	-150.08	-6.83	0.57	-28.37	-4.69
P4	-195.21	-6.29	-1.00	-59.43	-4.65
1b	-147.94	-10.63	-0.13	-38.52	-4.62
1c	-156.95	-12.12	-0.05	-39.49	-4.62
1d	-151.19	-11.98	-0.13	-40.69	-4.58
1n	-177.09	-6.68	-0.57	-26.16	-4.54
1l	-151.39	-9.55	-0.03	-28.60	-4.45

1

2

Figure 2

Docking of the 1,5-disubstituted tetrazole-1,2,3-triazoles with the protein Cov-2-M^{Pro}.

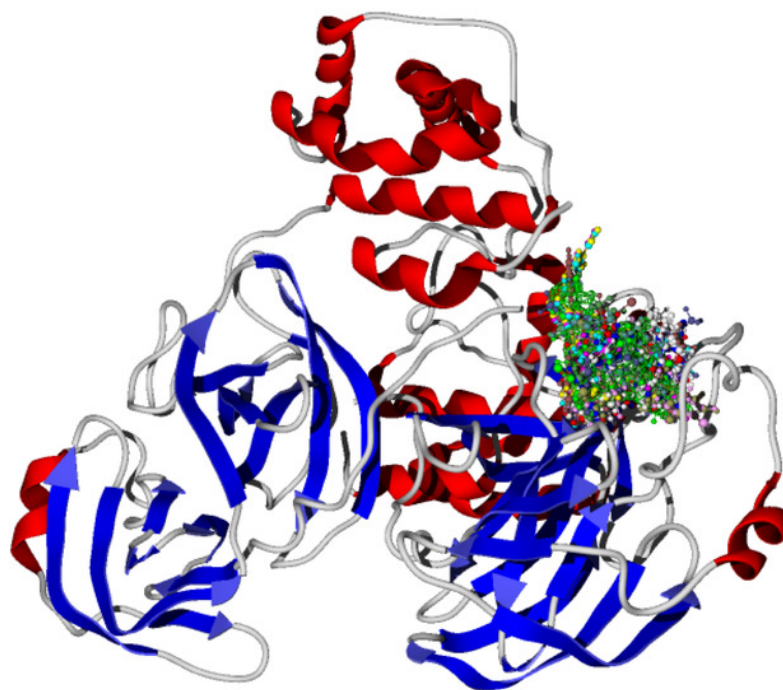


Figure 3

Catalytic site of the Cov-2-M^{Pro} protein

A) The co-crystallized ligand and B) the two best ligands interacting into the catalytic site of the Cov-2-M^{Pro} protein

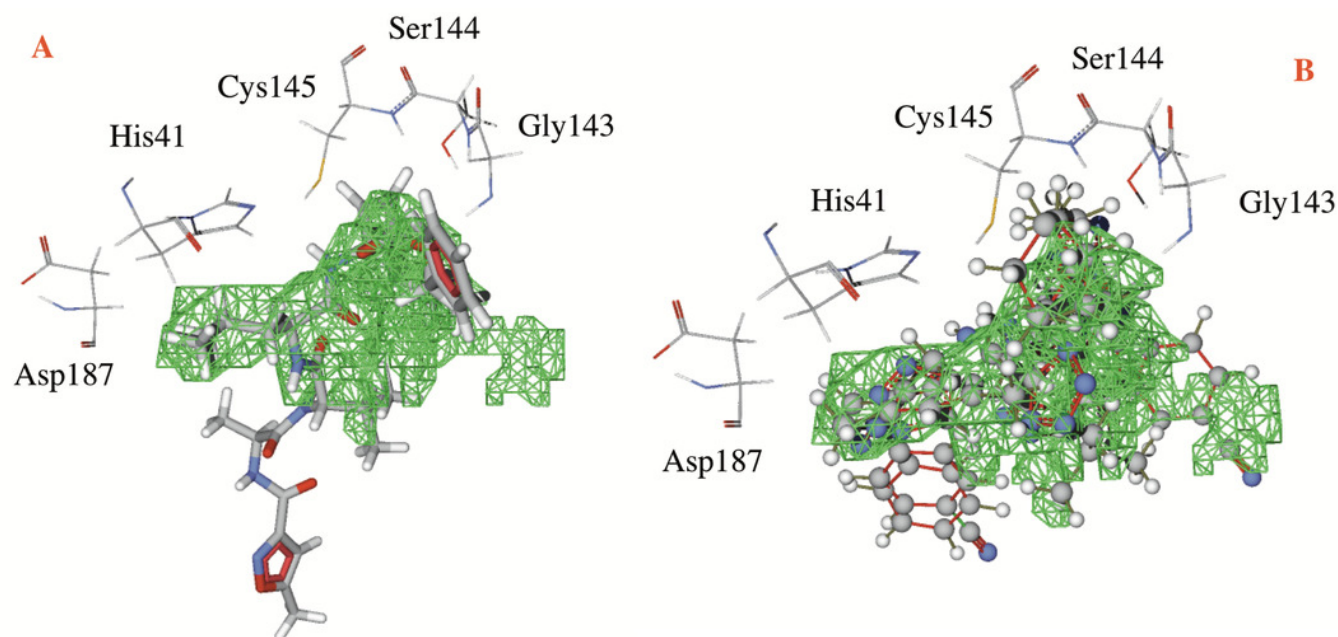


Figure 4

Hydrogen bond and electrostatic interactions between the Cov-2-M^{Pro} protein and the best ligand 1e.

Dotted blue lines represent the hydrogen bond interaction, as well as dotted green lines, represent the attractive electrostatic interactions and dotted red lines the repulsive electrostatic interactions.

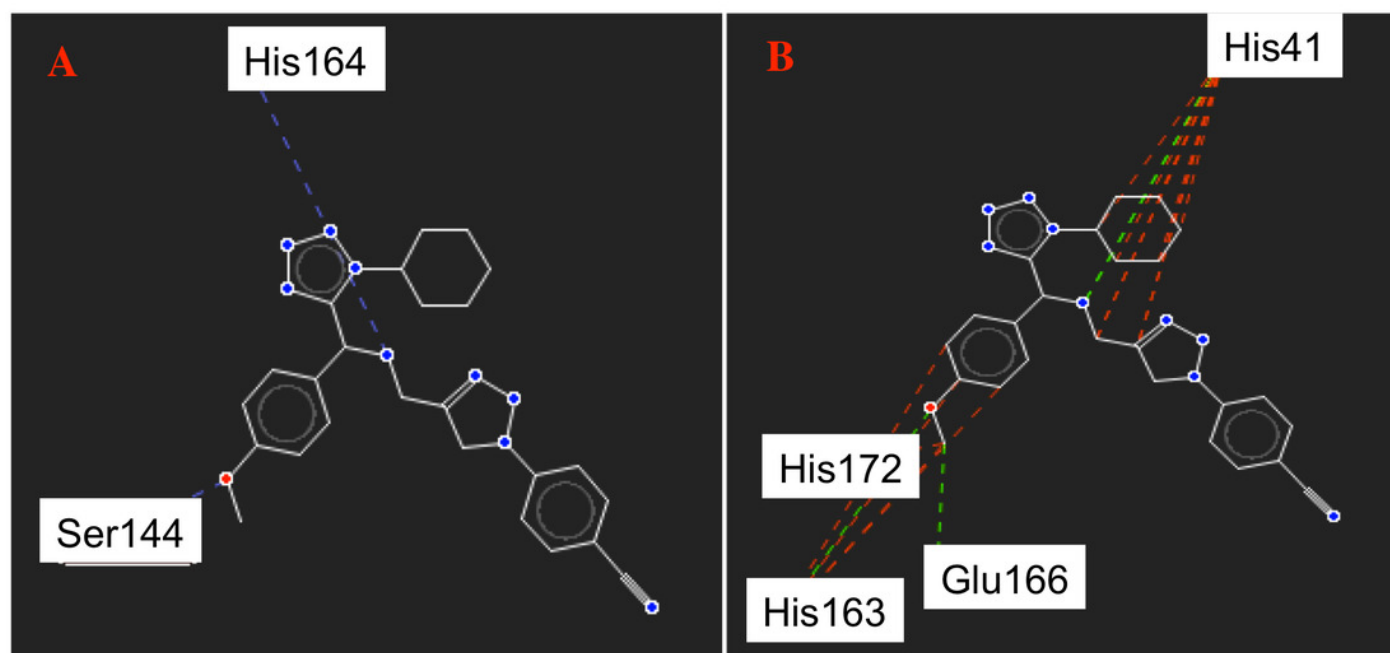


Figure 5

Hydrophobic interactions between the Cov-2-M^{Pro} protein and the main ligands

Hydrophobic interactions between the Cov-2-M^{Pro} protein and A) the co-crystallized ligand, and B) 1e. Blue surfaces represent hydrophobic sites, red surfaces are hydrophilic zones

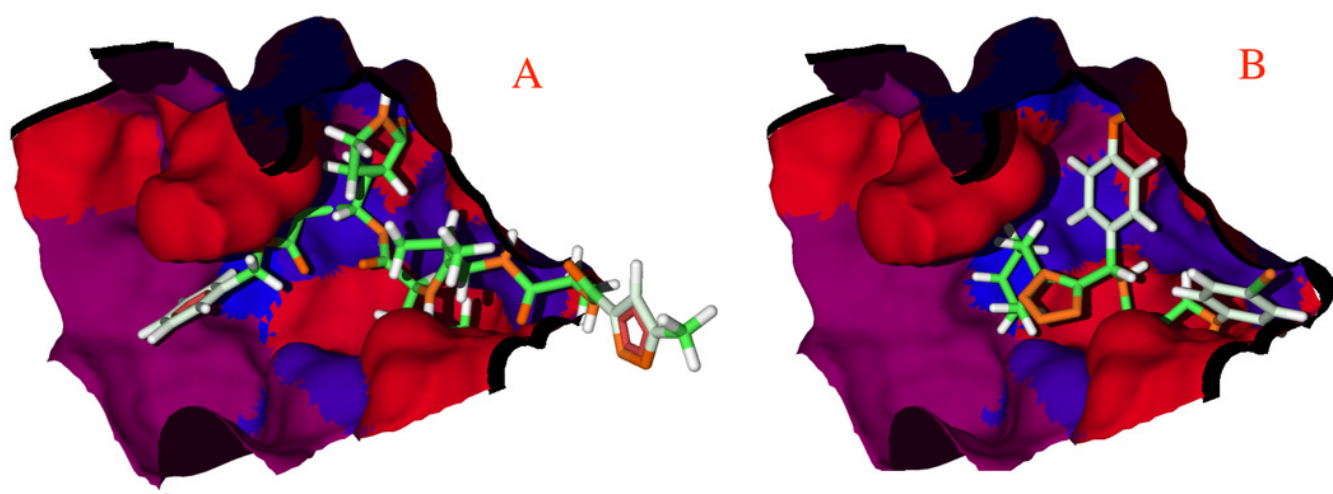


Figure 6

Pharmacophore model for the Cov-2-M^{Pro} protein

A) Front and B) lateral view for the pharmacophore model for the Cov-2-M^{Pro} protein. Green spheres depict the hydrophobic segments (Hy), blue spheres are the aromatic segments (Ar), purple spheres represent the hydrophobic and aromatic segments (Hy-Ar), gray spheres depict the hydrogen donor segments (HD) and the orange sphere represents the hydrogen acceptor segments (HA).

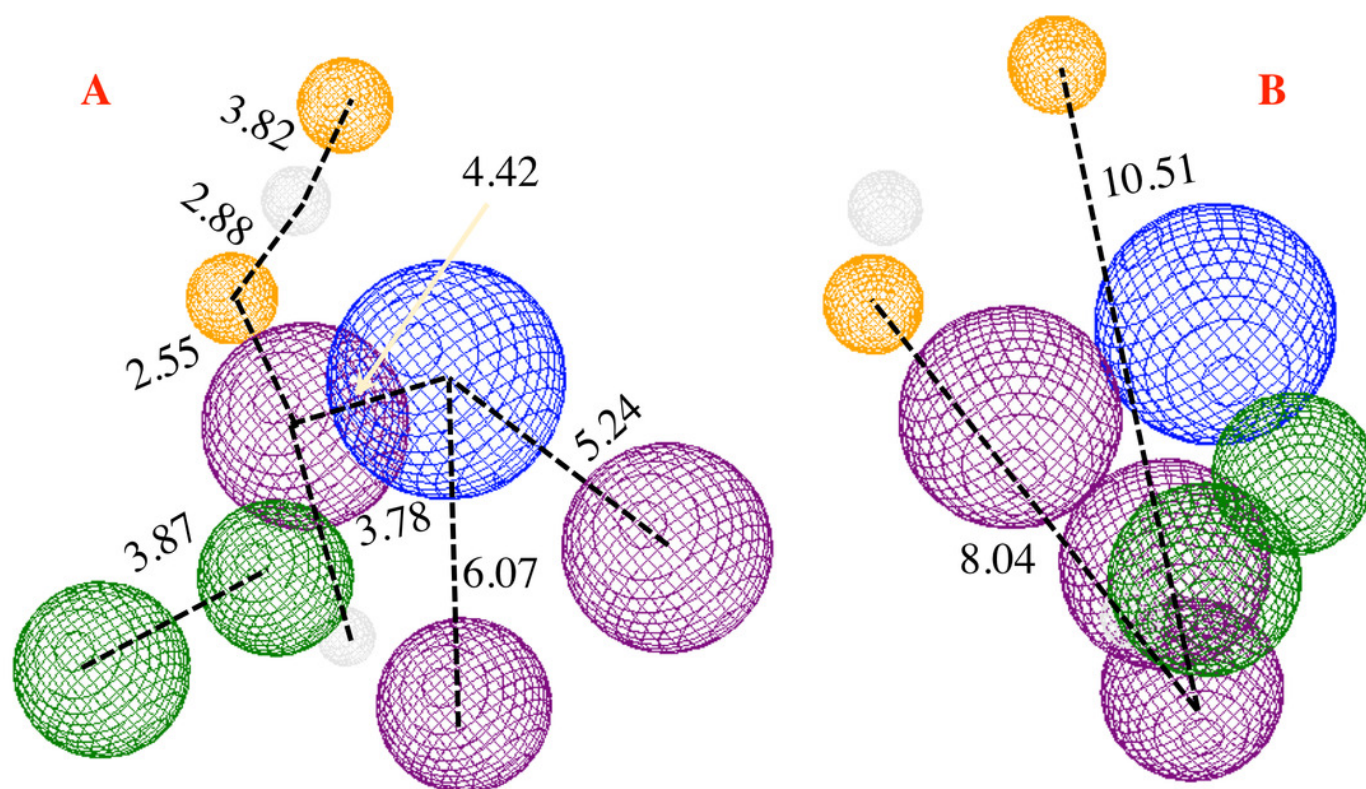


Figure 7

Designed compounds that present favorable interactions with the Cov-2-M^{Pro} protein.

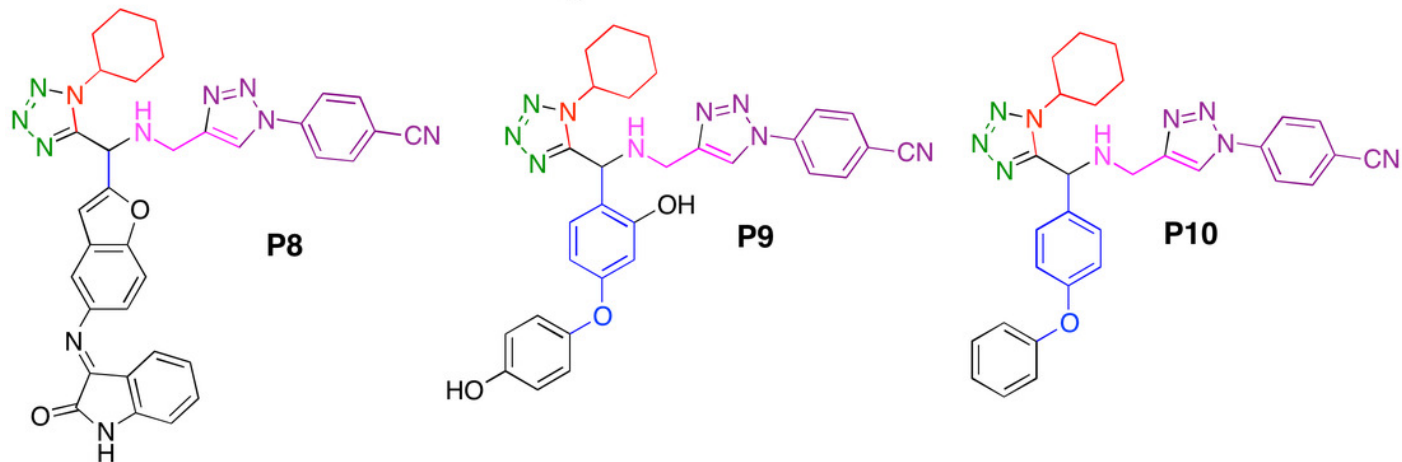
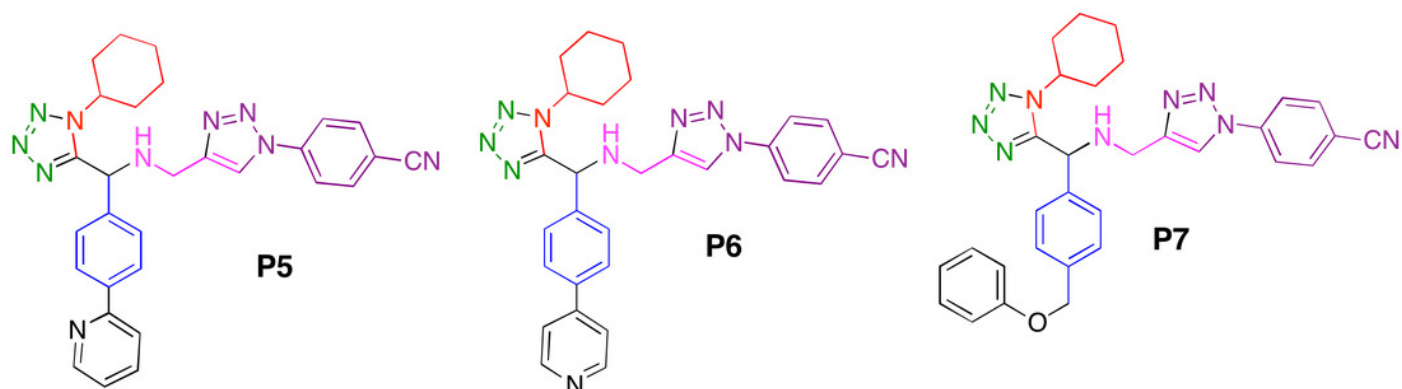
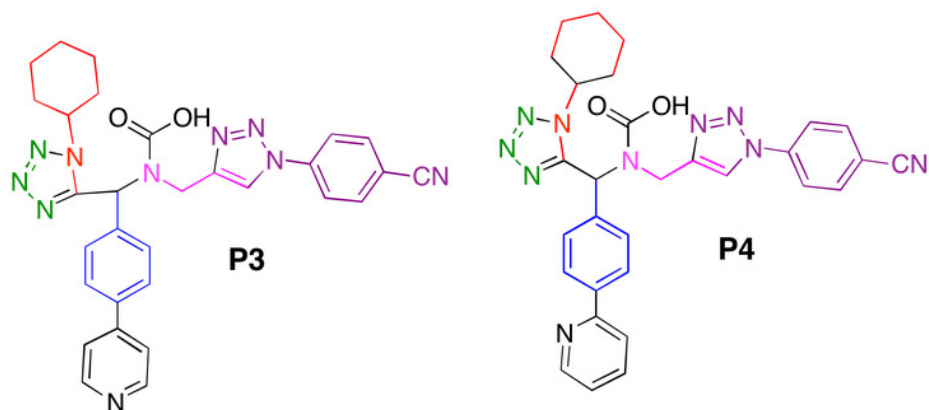
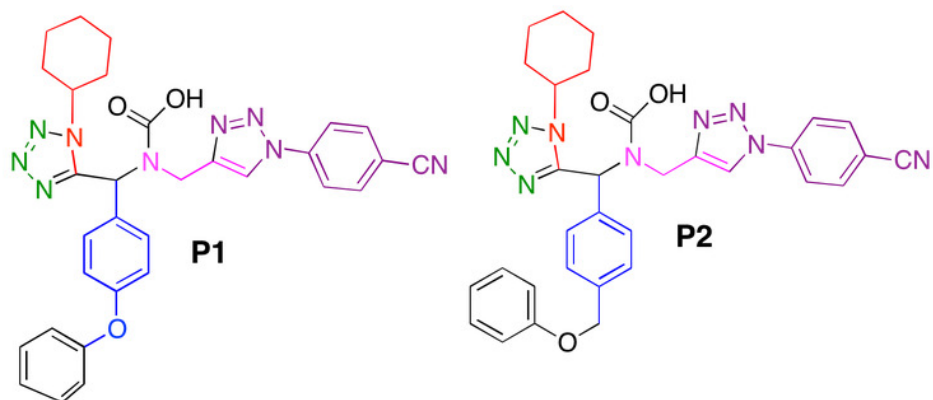


Figure 8

Non-covalent interactions between p8 and the Cov-2-M^{Pro} protein

A) Hydrophobic, B) Hydrogen bond and C) electrostatic interactions between p8 and the Cov-2-M^{Pro} protein. Blue surfaces represent hydrophobic sites, red surfaces are hydrophilic zones, dotted blue lines represent the hydrogen bond interactions, as well as the dotted green and red lines are the attractive and repulsive interactions, respectively.

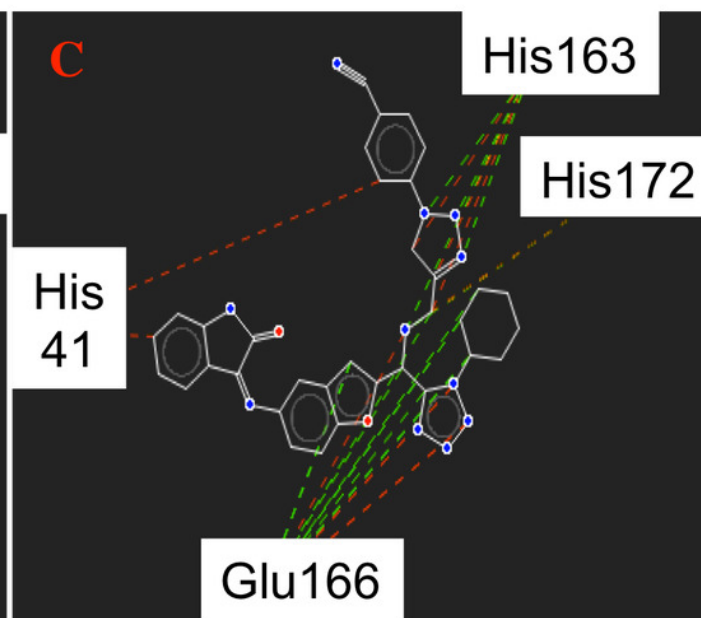
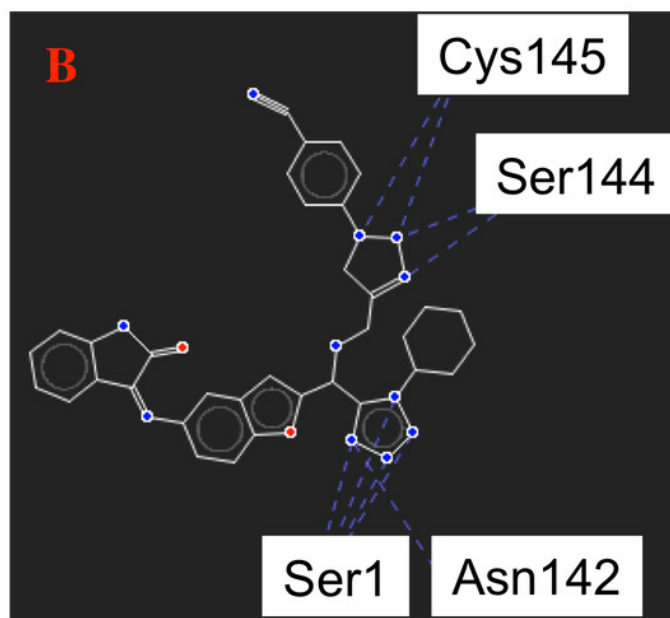
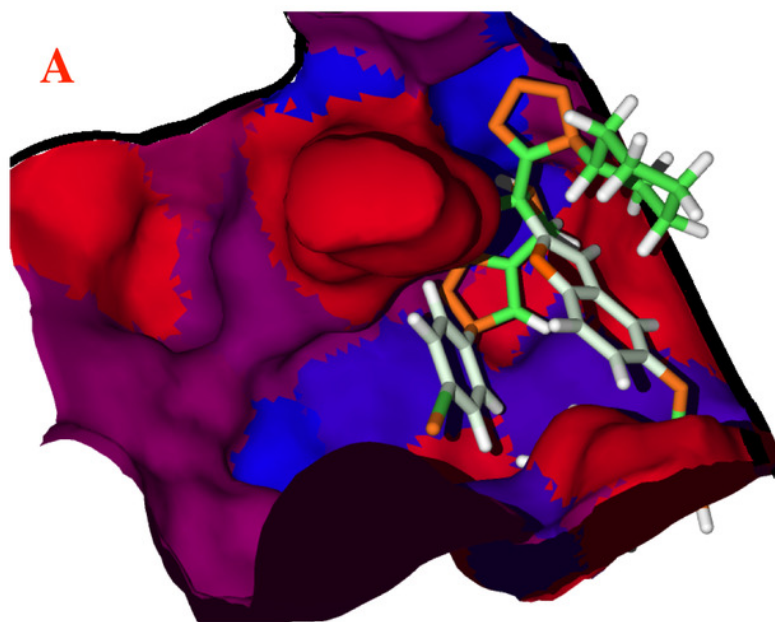


Figure 9

Main molecules overlap into the pharmacophore model for the Cov-2-M^{Pro} protein

A) 1e and B) p8 molecules overlap into the pharmacophore model for the Cov-2-M^{Pro} protein. Green spheres depict the hydrophobic segments (Hy), blue spheres are the aromatic segments (Ar), purple spheres represent the hydrophobic and aromatic segments (Hy-Ar), gray spheres depict the hydrogen donor segments (HD) and the orange sphere represents the hydrogen acceptor segments (HA).

